# FROZEN ORBITS FOR A SOLAR SAIL AROUND MERCURY

Eva Tresaco*, Jean Paulo S. Carvalho† and Antonio Elipe‡

**Solar sail is a new concept of spacecraft propulsion that uses solar radiation pressure to generate acceleration. This technology opens new and challenging possibilities to space-science missions such as deep-space exploration, space debris removal strategies and long term missions in the solar system. This article provides a method for finding initial conditions for frozen orbits around Mercury. Frozen orbits are those whose orbital elements remain constant on average. Thus, at a given latitude, the satellite always passes at the same altitude. This is very interesting for scientific missions that require close inspection of any celestial body. The orbital dynamics of the artificial satellite about Mercury is governed by the potential attraction of the main body and the gravity field of the third body (Sun). Besides the $J_2$ and $J_3$ secondary terms of the central body gravity field and the third body perturbation, our average model also includes the eccentricity and inclination of the orbit of the third body. We also take into account that the spacecraft is provided by a solar sail, in consequence the acceleration due to solar acceleration pressure is taken into consideration. In order to reduce the degrees of freedom of the dynamical system and remove short-period terms, a double averaging technique is applied. This algorithm is a two-fold process which firstly averages over the period of the satellite and secondly averages with respect to the period of the third body. This simplified Hamiltonian model is introduced in the Lagrange Planetary equations. Thus, frozen orbits are characterized by a surface depending on three variables: the orbital semi-major axis, eccentricity and inclination. Finally, the paper delves into the temporal evolution of the eccentricity of these orbits for different values of the sail area-to-mass ratio, which is a parameter related to the efficiency of the solar sail.**

## I. Introduction

THE use of propellantless propulsion systems like solar sails attract the interest for scientific missions. Solar sails offer new challenging space-science missions, they are considered for having artificial equilibrium points,[1–3] these displaced periodic orbits near libration points can be used, for example, as an alert of Geomagnetic storms.[4] They also make feasible new observation missions based on the computation of geocentric sun-synchronous frozen orbits.[5,6] On this latter issue we carry out this research, whose aim is the computation of frozen orbits for a solar sail.

Frozen orbits are orbits that have orbital elements constant on average. These orbits with constant mean eccentricity and argument of periapsis can be obtained as the equilibria of the averaged dynamical system. Actually, frozen orbits are very interesting for scientific missions because the control of the orbital eccentricity leads to the control of the spacecraft lifetime (see for instance Scheeres et al.,[7] Elipe et al.,[8,9] Carvalho et al.[10,11] and references therein).

The design of frozen orbits involves selecting the correct values of eccentricity and argument of periapsis, for a given semimajor axis and orbital inclination. Several procedures are used to find frozen orbits, from zeroing Gauss equations and solving the corresponding system, to the grid-method,[12] by Poincaré sections,[13] by numerical continuation of families of periodic orbits,[14] or by averaging the Hamiltonian and finding the equilibria of the reduced Hamiltonian. This last procedure is the one that we will use in this work; it has

*Associate Professor. Centro Universitario de la Defensa de Zaragoza and IUMA-Universidad de Zaragoza (Spain)

†Associate Professor. UFRB-Centro de Ciência e Tecnologia em Energia e Sustentabilidade, Universidade Federal do Recôcavo da Bahia (Brazil)

‡Professor. AIAA Associate Fellow. Centro Universitario de la Defensa de Zaragoza and IUMA-Universidad de Zaragoza (Spain)

been successfully used for finding frozen orbits for the zonal problem of an Earth artificial satellite,[15] of a satellite about the Moon,[16,17] around Europa,[11] around irregular asteroids[18,19] or with radiation pressure perturbation.[20]

In general, for orbiters around Mercury, it is necessary to consider the third-body attraction, that is, the Sun attraction, due to its proximity. If the spacecraft is provided with a large sail, the solar radiation pressure perturbation is worth considering. Thus, we deal with a Hamiltonian characterized by the Kepler problem, Mercury's gravitational potential, the third body perturbation and the solar radiation pressure. We also include the eccentricity and inclination of the orbit of Mercury around the Sun and the oblateness of Mercury caused by the zonal terms $J_2$ and $J_3$.

We give a brief description on the averaging techniques used in our work to reduce the dynamical problem to only one degree of freedom system. Then, we obtain the equilibria characterized by a surface depending on three variables, namely semi-major axis, eccentricity and inclination, which points will correspond to frozen orbits. We shall see that the contribution of each perturbation term depends on the altitude of the orbits in such a way that, for low-altitude orbits, the influence of the third body is almost negligible and consequently and we could approach this problem using the zonal problem. However, for moderate altitudes we need to cope with all the terms. Finally, let us remark that the frozen orbits computed are no longer frozen when we include more complex force functions in the dynamical model. Hence, the averaged initial conditions from a simplified model may be used as starters of numerical correction procedures in order to have frozen orbits for the more complete model.[16,21]

## II. Dynamical model

We consider the motion of an orbiter around Mercury under its gravitational force and the third body attraction due to the Sun. We are not under the Hill hypothesis, Mercury orbit around the Sun is clearly eccentric and it also exhibits a certain inclination (see Table 1), so we will study both the planar and inclined case of the third body. Because Mercury has a known oblateness we also include both $J_2$ and $J_3$ harmonics coefficients of Mercury's gravitational potential.

Let us consider a $Oxyz$ reference frame centered on the main body, Mercury, the $Oxy$ plane coincides with the planet's equator, the $x$-axis along the intersection line of the equatorial plane of the main body and the orbital plane of the third body, see Figure 1. It is assumed that the third body follows an elliptic inclined orbit around the main body with semimajor axis $a_\odot$, eccentricity $e_\odot$ and inclination $i_\odot$. The spacecraft orbits about the central body with semimajor axis $a$, eccentricity $e$, inclination $i$, right ascension of the ascending node $\Omega$, argument of the periapsis $w$ and mean motion $n$, and its motion is perturbed by the third body.

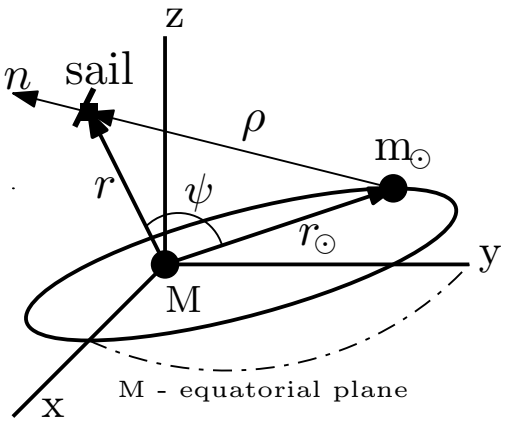


**Figure 1. Scheme of the dynamical system.**

The equation of motion of the spacecraft is given by

$$\ddot{\mathbf{r}} = \ddot{\mathbf{r}}_{\mathbf{M}} + \ddot{\mathbf{r}}_{\mathbf{3b}}, \tag{1}$$

where $\ddot{\mathbf{r}}_{\mathbf{M}}$ is the force induced by Mercury gravity field, which can be expressed as the gradient of a certain potential $U_M$ in terms of the position of the state vector $\mathbf{r}$ of the spacecraft with respect to the central planet

| | | | |
|---|---|---|---|
| Sun | $\mu_\odot = 132712442099\,[\mathrm{km}^3/\mathrm{s}^2]$ | | |
| Mercury | $\mu = 22032.09\,[\mathrm{km}^3/\mathrm{s}^2]$ | $R_M = 2439.7[\mathrm{km}]$ | $J_2 = 6 \times 10^{-5}$ |
| Mercury orbit | $a_\odot = 5.79 \times 10^7[\mathrm{km}]$ | $e_\odot = 0.20563593$ | $i_\odot = 7.00559432\,^\circ$ |

**Table 1. Parameters of the dynamical model.**

Mercury,

$$\ddot{\mathbf{r}}_{\mathbf{M}} = \nabla U_M(\mathbf{r}). \tag{2}$$

The term $\ddot{\mathbf{r}}_{\mathbf{3b}}$ is the resultant of the gravitation attraction of the third body (Sun) and can be expressed with respect to Mercury's centre of mass

$$\ddot{\mathbf{r}}_{\mathbf{3b}} = -\mu_\odot \left( \frac{\mathbf{r} - \mathbf{r}_\odot}{\|\mathbf{r} - \mathbf{r}_\odot\|^3} + \frac{\mathbf{r}_\odot}{\|\mathbf{r}_\odot\|^3} \right), \tag{3}$$

where $\mu_\odot$ represents the gravitational parameter of the Sun (its value is given in Table 1), and $\mathbf{r}_\odot$ is the position vector of the Sun with respect to Mercury.

If the spacecraft is provided with a large sail it is necessary to add to Eq. (1) the acceleration generated by the solar radiation pressure,

$$\ddot{\mathbf{r}} = \ddot{\mathbf{r}}_{\mathbf{M}} + \ddot{\mathbf{r}}_{\mathbf{3b}} + \ddot{\mathbf{r}}_{\mathbf{SRP}}.$$

The idea of using a solar sail is to take advantage of the solar radiation pressure, in this way the sail experiences a small but unlimited and continuous acceleration. The solar radiation pressure is added as source of orbital perturbation.
The pressure $P$ exerted on the sail by the solar radiation can be expressed in terms of the energy flux $W$ divided by the speed of light $c$,

$$P = \frac{W}{c}. \tag{4}$$

The energy flux $W$ is the flux per unit of area, it can be written in terms of the Sun's luminosity, $L_\odot$, and the distance from the Sun, $r_{s\odot}$,

$$W = \frac{L_\odot}{4\pi r_{s\odot}^2}. \tag{5}$$

We consider a perfectly reflecting sail, i.e. photons emitted by the Sun that impact on the sail are totally reflected, thus the pressure is twice its value. We also assume that the force on the sail is exerted normal to its surface, see Figure (2) (details can be found in[22]).

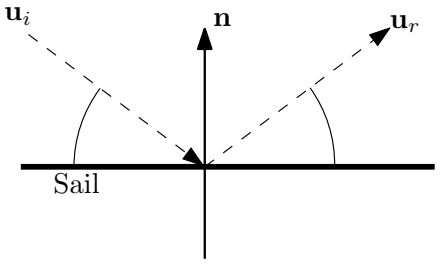


**Figure 2. Scheme of a perfect sail (flat and 100% reflection).**

Therefore, the solar sail acceleration is expressed as

$$\ddot{\mathbf{r}}_{SRP} = \frac{L_S}{c\,2\pi\rho^2}\,\frac{A}{m}\,(\mathbf{u}_i \cdot \mathbf{n})^2\mathbf{n}, \tag{6}$$

where $m$ is the mass of the spacecraft. We will assume that the sail maintains a fixed orientation perpendicular to the Sun line ($\mathbf{u}_i \| \mathbf{n}$), then the sail effect takes its maximum value $(\mathbf{u}_i \cdot \mathbf{n}) = 1$. The solar sail

acceleration, given in Equation (6) in terms of the area-to-mass ratio $A/m$ of the sail, is also expressed in terms of the lightness number of the sail, $\beta$, a dimensionless ratio of the solar radiation pressure acceleration to the solar gravitational acceleration that measures the effectiveness of the sail. It is defined as

$$\beta = \frac{\sigma^*}{\sigma},$$

where $\sigma^* = \dfrac{L_S}{c\,2\pi\mu_\odot} = 1.53\,[\mathrm{gr/m^2}]$ , and $\sigma$ is the sail loading parameter (areal density) given by the total mass of the spacecraft divided by the sail area, $\sigma = m/A$ expressed in $[\mathrm{gr/m^2}]$.
Thus, taking into account that the sail is assumed to maintain the orientation perpendicular to the Sun line $\mathbf{n} = \rho/\|\rho\|$, and the sail is located at distance from the Sun $\rho = \|\mathbf{r} - \mathbf{r}_\odot\|$, the solar radiation pressure due to a flat sail fixed perpendicular to the Sun line is given by

$$\ddot{\mathbf{r}}_{SRP} = \beta\,\mu_\odot \frac{\mathbf{r} - \mathbf{r}_\odot}{\|\mathbf{r} - \mathbf{r}_\odot\|^3}. \tag{7}$$

Note that the force on a solar sail depends on the sail's area and orientation. When the perturbation term due to solar radiation pressure is added the system, it only holds its Hamiltonian character when the sail is aligned with respect to the Sun, i.e., no sail effect, or in the case that the sail is perpendicular to the Sun-sail direction, i.e., maximum sail effect. For other sail orientations the systems is no longer Hamiltonian.

As it is stated above, perturbation due to solar radiation pressure depends strongly on the sail size and mass and the orbit altitude, thus we will range the area-to-mass coefficient of the satellite and its altitude in order to visualize their impact on the sail dynamics.

### A. Hamiltonian description

The motion of the solar sail about Mercury under the gravitational effect of the central body and perturbed by the gravitational attraction of the third body, Sun, and the Solar radiation pressure is described by

$$\ddot{\mathbf{r}} = \ddot{\mathbf{r}}_{\mathbf{M}} + \ddot{\mathbf{r}}_{\mathbf{3b}} + \ddot{\mathbf{r}}_{\mathbf{SRP}} = \nabla U_M(\mathbf{r}) - \mu_\odot \left( \frac{\mathbf{r} - \mathbf{r}_\odot}{\|\mathbf{r} - \mathbf{r}_\odot\|^3} + \frac{\mathbf{r}_\odot}{\|\mathbf{r}_\odot\|^3} \right) + \beta\,\mu_\odot \frac{\mathbf{r} - \mathbf{r}_\odot}{\|\mathbf{r} - \mathbf{r}_\odot\|^3}, \tag{8}$$

Hence, the Hamiltonian is

$$\mathcal{H} = \frac{1}{2}(\dot{\mathbf{r}} \cdot \dot{\mathbf{r}}) - (U_M + U_{3b} + U_{SRP}), \tag{9}$$

where, for the central planet, we only take into account the zonal contribution,

$$U_M = \frac{\mu}{r} - \frac{\mu}{r} \sum_{n \geq 2} \left( \frac{R_M}{r} \right)^n J_n P_n(\sin\phi), \tag{10}$$

$r$ is the distance from the sail to the central planet: $r = \|\mathbf{r}\|$, $R_M$ is the equatorial radius of Mercury (see Table (1)) and $\phi$ is the latitude of the sail orbit with respect to the equatorial plane of Mercury. Using spherical trigonometry we have $\sin\phi = \sin i \sin(w + f)$, where $f$ is the true anomaly of the sail, $i$ the orbital inclination, $w$ the argument of the periapsis and $P_n(x)$ the Legendre polynomial of order $n$. We only consider the harmonics coefficients $J_2$ and $J_3$; the corresponding Legendre polynomials are

$$P_2(\sin\phi) = \frac{1}{2}\left(3s^2 \sin^2(w+f) - 1\right), \quad P_3 = \frac{1}{2}\left(5s^3 \sin^3(w+f) - 3s\sin(w+f)\right),$$

with the shortcuts $s = \sin i$, $c = \cos i$. After some trigonometric manipulations we get that the perturbation due to the $J_2$ term, we named $R_{J_2}$, is given by

$$R_{J_2} = \frac{\mu\,R_M^2\,J_2}{4r^3}\Big(1 - 3c^2 - 3s^2\cos(2w + 2f)\Big), \tag{11}$$

and the perturbation caused by the "pear shape" of the central body, $J_3$ term, is

$$R_{J_3} = -\frac{\mu\,R_M^3\,J_3}{8r^4}s\Big(3\sin(w+f) - 5\sin(3w+3f) + 5c^2\sin(3w+3f) - 15c^2\sin(w+f)\Big). \tag{12}$$

If we look at the gravitational acceleration due to the third body (Eq. (8)), the potential function is

$$U_{3b} = \mu_\odot \left( \frac{1}{\|\mathbf{r} - \mathbf{r}_\odot\|} - \frac{\mathbf{r} \cdot \mathbf{r}_\odot}{r_\odot^3} \right), \tag{13}$$

where $r_\odot = \|\mathbf{r}_\odot\|$. Since we are interested in the case $r \ll r_\odot$, the first summand is expanded as a series of Legendre polynomials up to second order,

$$\frac{1}{\|\mathbf{r} - \mathbf{r}_\odot\|} = \frac{1}{r_\odot} \left( 1 - 2\frac{r}{r_\odot} \cos\psi + \left(\frac{r}{r_\odot}\right)^2 \right)^{-1/2} = \frac{1}{r_\odot} \sum_{n \geq 0}^{2} \left( \frac{r}{r_\odot} \right)^n P_n(\cos\psi).$$

By the replacing the expressions of the Legendre polynomials $P_0(\cos\psi) = 1$, $P_1(\cos\psi) = \cos\psi$, and $P_2(\cos\psi) = (-1 + 3\cos^2\psi)/2$, the second summand of Eq. (13) cancels with the $P_1$ term, then we have

$$U_{3b} = \frac{\mu_\odot}{r_\odot} \left( 1 + \frac{1}{2} \left( \frac{r}{r_\odot} \right)^2 (3\cos^2\psi - 1) \right). \tag{14}$$

Considering the solar radiation acceleration, we show that if we assume the case of a solar sail always perpendicular to the Sun-sail direction, the Sun gravitational attraction and the sail acceleration are equal in magnitude but in opposite directions. Hence, the sail acceleration due to the radiation pressure can be expressed as the gradient of the following potential

$$U_{SRP} = -\beta\mu_\odot \left( \frac{1}{\|\mathbf{r} - \mathbf{r}_\odot\|} \right). \tag{15}$$

Based on the procedure followed for the third body perturbation, this potential function can be expanded in terms of Legendre polynomials up to the second order; note that $P_0(\cos\psi)$ is omitted because it does not depend on the orbital elements of the sail, but $P_1(\cos\psi)$ term is not eliminated in this case.

$$U_{SRP} = -\beta\frac{\mu_\odot}{r_\odot} \left( 1 + \frac{r}{r_\odot} \cos\psi + \frac{1}{2} \left( \frac{r}{r_\odot} \right)^2 (3\cos^2\psi - 1) \right). \tag{16}$$

On the other hand, the angle $\psi$ is the angle between radius vectors $\mathbf{r}$ and $\mathbf{r}_\odot$ (see Fig.(1)), which can be expressed in terms of the orbital elements of the third body and the spacecraft,

$$\cos\psi = \frac{\mathbf{r} \cdot \mathbf{r}_\odot}{r\, r_\odot},$$

where

$$\frac{\mathbf{r}}{r} = \begin{pmatrix} \cos\Omega\cos(w+f) - \sin\Omega\sin(w+f)\cos i \\ \sin\Omega\cos(w+f) + \cos\Omega\sin(w+f)\cos i \\ \sin(w+f)\sin i \end{pmatrix}$$

and

$$\frac{\mathbf{r}_\odot}{r_\odot} = \begin{pmatrix} \cos\Omega_\odot\cos f_\odot - \sin\Omega_\odot\sin f_\odot\cos i_\odot \\ \sin\Omega_\odot\cos f_\odot + \cos\Omega_\odot\sin f_\odot\cos i_\odot \\ \sin f_\odot \sin i_\odot \end{pmatrix}.$$

We have assumed $w_\odot = 0$ without loss of generality because it is cancelled when the second average over the period of the third body is performed.

Using this mathematical relation between the angle $\psi$ and the true anomaly of the sail, and after some algebraic manipulations, we can write

$$\cos\psi = \alpha\cos f + \gamma\sin f,$$

where coefficients $\alpha$ and $\gamma$ depend on the right argument of the ascending node, argument of the periapsis and true anomaly of both the sail and the third body.

$$\alpha = \cos w\cos(\Omega - \Omega_\odot)\cos f_\odot + \sin i\sin i_\odot\sin w\sin f_\odot + \cos w\cos i_\odot\sin(\Omega - \Omega_\odot)\sin f_\odot$$

$$- \sin w\cos i\sin(\Omega - \Omega_\odot)\cos f_\odot + \sin w\cos i\cos i_\odot\cos(\Omega - \Omega_\odot)\sin f_\odot.$$

$$\begin{aligned}\gamma = &-\sin w\cos(\Omega-\Omega_\odot)\cos f_\odot + \sin i\sin i_\odot\cos w\sin f_\odot - \sin w\cos i_\odot\sin(\Omega-\Omega_\odot)\sin f_\odot \\ &-\cos w\cos i\sin(\Omega-\Omega_\odot)\cos f_\odot + \cos w\cos i\cos i_\odot\cos(\Omega-\Omega_\odot)\sin f_\odot.\end{aligned} \tag{17}$$

Thus, the disturbing function due to the third body perturbation, named $R_{3b}$, is

$$R_{3b} = \frac{\mu_\odot}{2r_\odot}\left(\frac{r}{r_\odot}\right)^2\left(3(\alpha\cos f+\gamma\sin f)^2-1\right), \tag{18}$$

and the disturbing function due to solar radiation pressure is

$$R_{SRP} = -\beta\left(\mu_\odot\frac{r}{r_\odot^2}\cos\psi + \frac{\mu_\odot}{2r_\odot}\left(\frac{r}{r_\odot}\right)^2\left(3(\alpha\cos f+\gamma\sin f)^2-1\right)\right), \tag{19}$$

where $P_0$ term has been dropped from the Hamiltonian because it is independent of the orbital elements of the spacecraft.

Summarizing, for the model considered in this study the perturbing function is given by the addition of the stated perturbation equations

$$R_{J2} + R_{J_3} + R_{3b} + R_{SRP}. \tag{20}$$

depicted in Eq. (11), Eq. (12), Eq. (18) and Eq. (19).

## III. Averaging techniques

We present an analytical procedure using an averaged model in order to focus on the computation of frozen orbits. We are not interested in developing a complete analytical theory but to help in mission design, where frozen orbits are of major interest. Frozen orbits are those that keep their orbital eccentricity and argument of periapsis constant on average. Therefore, the motion of the sail is studied under the double-averaged analytical model with the aim of reducing the degrees of freedom of the system and eliminate the short-period terms. The double averaged algorithm is a two-fold process which firstly averages over the period of the satellite and secondly averages with respect to the period of the third body. The standard definition for average a certain function $F$ is

$$\langle F\rangle = \frac{1}{2\pi}\int_0^{2\pi} F\ dM, \tag{21}$$

where $M$ stands for the mean anomaly.

### A. First average

First, we perform an average over the eccentric anomaly of the spacecraft using the known relations of elliptic motion

$$dM = (1-e\cos E)dE, \quad \frac{r}{a} = 1-e\cos E, \quad \sin f = \frac{\sqrt{1-e^2}\sin E}{1-e\cos E}, \quad \cos f = \frac{e-\cos E}{1-e\cos E}.$$

Applying these equation to the perturbation functions due to the non-sphericity of the primary body, Eq. (11) and Eq. (12), we get the following averaged potential induced by the Mercury's gravity field

$$\begin{aligned}\langle R_{J_2}\rangle &= -\frac{1}{4}R_M^2\,J_2\frac{n^2(-2+3\sin^2 i)}{(1-e^2)^{3/2}}, \\ \langle R_{J_3}\rangle &= -\frac{3}{8}R_M^3\,J_3\frac{n^2\,e\,\sin i\sin w(-4+5\sin^2 i)}{a(1-e^2)^{5/2}}.\end{aligned} \tag{22}$$

which describe the secular perturbation of the motion of a spacecraft due to the harmonics $J_2$ and $J_3$. Now we need to average the term given in Eq. (18) that corresponds to the disturbing body, the Sun. We multiply

and divide that equation by $a/a_\odot$ to solve the average integral using the well-known relations between orbital elements. After performing the average over the eccentric anomaly of the sail, the equation obtained is

$$\langle R_{3b}\rangle = \frac{3a^2 n_\odot^2}{4}\left(\frac{a_\odot}{r_\odot}\right)^3\left(\alpha^2(1+4e^2)+\gamma^2(1-e^2)-(\frac{2}{3}+e^2)\right), \tag{23}$$

where $n_\odot$ is the mean motion of the third body.

Regarding to solar radiation pressure perturbation, we average Eq. 19 over the eccentric anomaly of the spacecraft and we obtain the following expression

$$\langle R_{SRP}\rangle = -\beta\frac{3a^2 n_\odot^2}{4}\left(\frac{a_\odot}{r_\odot}\right)^3\left(\alpha^2(1+4e^2)+\gamma^2(1-e^2)-(\frac{2}{3}+e^2)+\frac{2\alpha\, e\, r_\odot}{a}\right), \tag{24}$$

### B. Second average

Second average is applied with respect to the third body perturbation. To do this, we perform an average over the true anomaly of the disturbing body, $f_\odot$. We use the previous relations between the orbital elements, expressed in terms of the third body, in addition with the following

$$\frac{r_\odot}{a_\odot} = \frac{1-e_\odot^2}{1+e_\odot\,\cos f_\odot}, \quad dM_\odot = \frac{r_\odot^2}{a_\odot^2\sqrt{1-e_\odot^2}}\,df_\odot.$$

Note that the orbital elements of the spacecraft are constant during this averaging process, thus

$$\langle\langle R_{J_2}\rangle\rangle = \langle R_{J_2}\rangle, \quad \langle\langle R_{J_3}\rangle\rangle = \langle R_{J_3}\rangle \tag{25}$$

When we apply the average over the period of the disturbing body we get the following expression

$$\langle\langle R_{3b}\rangle\rangle \;=\; \frac{3a^2 n_\odot^2}{4\left(1-e_\odot^2\right)^{3/2}}\Big(\frac{\alpha_1^2+\alpha_2^2}{2}(1+4e^2)+\frac{\gamma_1^2+\gamma_2^2}{2}(1-e^2)-(\frac{2}{3}+e^2)\Big). \tag{26}$$

where we have rewritten $\alpha$ and $\gamma$ given in Eq.17 as $\alpha = \alpha_1\cos f_\odot + \alpha_2 \sin f_\odot$ and $\gamma = \gamma_1\cos f_\odot + \gamma_2 \sin f_\odot$, with

$$\begin{aligned}
\alpha_1 &= \cos w\cos(\Omega-\Omega_\odot) - \sin w\cos i\sin(\Omega-\Omega_\odot),\\
\alpha_2 &= \sin i\sin i_\odot\sin w + \cos w\cos i_\odot\sin(\Omega-\Omega_\odot) + \sin w\cos i\cos i_\odot\cos(\Omega-\Omega_\odot),\\
\gamma_1 &= -\sin w\cos(\Omega-\Omega_\odot) - \cos w\cos i\sin(\Omega-\Omega_\odot),\\
\gamma_2 &= \sin i\sin i_\odot\cos w - \sin w\cos i_\odot\sin(\Omega-\Omega_\odot) + \cos w\cos i\cos i_\odot\cos(\Omega-\Omega_\odot).
\end{aligned} \tag{27}$$

For the solar radiation pressure perturbation, the last summand of its potential function given in equation Eq. (24) is canceled after the average over the third body period. Hence, we get the same expression than $\langle\langle R_{3b}\rangle\rangle$ but multiplied by $-\beta$,

$$\langle\langle R_{SRP}\rangle\rangle \;=\; -\beta\frac{3a^2 n_\odot^2}{4\left(1-e_\odot^2\right)^{3/2}}\Big(\frac{\alpha_1^2+\alpha_2^2}{2}(1+4e^2)+\frac{\gamma_1^2+\gamma_2^2}{2}(1-e^2)-(\frac{2}{3}+e^2)\Big). \tag{28}$$

Subsequently, for the case of a solar sail with fixed orientation perpendicular to the sun-sail direction, the double-averaging transformations applied to the solar radiation perturbation produces

$$\langle\langle R_{SRP}\rangle\rangle = -\beta\,\langle\langle R_{3b}\rangle\rangle. \tag{29}$$

Thus, the secular disturbing potential of the orbital motion of a sail orbiting Mercury when we take into account the zonals of the planet and the gravitational attraction of the Sun and solar radiation pressure, is the addition of the preceding perturbation terms, named $R$

$$R = \langle\langle R_{J2}\rangle\rangle + \langle\langle R_{J_3}\rangle\rangle + (1-\beta)\langle\langle R_{3b}\rangle\rangle. \tag{30}$$

## IV. Frozen orbits

In order to analyze the effect of the disturbing potential on the orbital elements of the spacecraft, the double-averaged potential (Eq. (30)) is replaced in the Lagrange's planetary equations that describe the temporal variation of the orbital elements. We are interested in frozen orbits, which are characterized by no secular terms in eccentricity and argument of the periapsis. Frozen orbits are orbits of consideration for mission planning purposes because they maintain almost constant altitude and require small amounts of fuel for orbital maintenance. The variation of the eccentricity and argument of periapsis is given by their corresponding Lagrange's equations:

$$\begin{aligned}\frac{dw}{dt} &= \frac{-\sqrt{1-e^2}}{n\,a^2 e}\,\frac{\partial R}{\partial e} + \frac{\cot i}{n\,a^2\sqrt{1-e^2}}\,\frac{\partial R}{\partial i},\\ \frac{de}{dt} &= \frac{\sqrt{1-e^2}}{n\,a^2 e}\,\frac{\partial R}{\partial w} - \frac{1-e^2}{n\,a^2\,e}\,\frac{\partial R}{\partial M}.\end{aligned} \tag{31}$$

Frozen orbits are identified as the equilibrium points of these equations, therefore the final stage is undertaken by solving the equations

$$\frac{dw}{dt} = 0, \quad \frac{de}{dt} = 0. \tag{32}$$

Let us replace on the previous system the reduced potential $R$ (Eq. (30)).

$$\begin{aligned}\frac{dw}{dt} &= -J_2\,\frac{3R_M^2 n(5\cos 2i+3)}{8a^2(e^2-1)^2} - J_3\,\frac{3R_M^3 n\csc i\sin w\left(5(7e^2+1)\cos 4i - 3e^2 - 4\cos 2i - 1\right)}{64a^3 e(e^2-1)^3}\\ &+(1-\beta)\Bigg[-\frac{3n_\odot^2\sqrt{1-e^2}}{4n\left(1-e_\odot^2\right)^{3/2}}\Big(4(\alpha_1^2+\alpha_2^2)-(\gamma_1^2+\gamma_2^2)-\frac{4}{3}\Big)\\ &+\frac{3\,n_\odot^2\,\cot i}{4n\sqrt{1-e^2}\left(1-e_\odot^2\right)^{3/2}}\Big((1+4e^2)\Big(\alpha_1\frac{\partial\alpha_1}{\partial i}+\alpha_2\frac{\partial\alpha_2}{\partial i}\Big)+(1-e^2)\Big(\gamma_1\frac{\partial\gamma_1}{\partial i}+\gamma_2\frac{\partial\gamma_2}{\partial i}\Big)\Big)\Bigg],\end{aligned} \tag{33}$$

$$\frac{de}{dt} = -J_3\,\frac{3R_M^3 n^2\,e\,\sin i\cos w(-4+5\sin^2 i)}{8a(1-e^2)^{5/2}} + (1-\beta)\frac{15\,n_\odot^2\,e\,\sqrt{1-e^2}}{4n\left(1-e_\odot^2\right)^{3/2}}\Big(\alpha_1\gamma_1+\alpha_2\gamma_2\Big). \tag{34}$$

The derivative terms $\partial\alpha_1/\partial i,\ldots$ can be easily obtained through the partial differentiation of Eq. (27). Note that the second equation $de/dt = 0$, Eq. (34), clearly holds when $\cos w = 0$ if the third body orbit is planar ($i_\odot = 0$). While, in the case of inclined third body, $i_\odot \neq 0$, it is required that both $\sin(\Omega - \Omega_\odot) = 0$ and $\cos w = 0$. That is, we will search frozen orbits for $w = \pi/2$ and $w = 3\pi/2$ and $\Omega - \Omega_\odot = 2k\pi$, $k \in \mathbb{Z}$. Hence, equation $dw/dt = 0$ depends on three variables, namely, eccentricity $e$, inclination $i$, and semimajor axis $a$. This equation represents a surface; points on this surface correspond to equilibria of the system given in Eq. (32), that is, points on the surface

$$\mathcal{F}(a,e,i) \equiv \frac{d}{dt}w(a,e,i) = 0$$

correspond to initial conditions $(a,e,i)$ of frozen orbits.

Now we present some examples for different values of parameters of the radiation pressure coefficient $\beta$ and $J_3$. All constants but $J_3$ are given in Table 1. This zonal harmonic reflects an asymmetry between both hemispheres of Mercury and influences the orbital altitude at pericenter. Recent Messenger mission (2011) provided new accurate data about the gravity field coefficients,[23] thus the $J_3$ coefficient in the HgM002 gravity model for Mercury is $J_3 = J_2/5$. Previous works[24,25] analyze the phase space for different values of $J_3$ equal to $\pm J_2/2, \pm J_2/10$. Note that the sign of $J_3$ is connected to the term "$\sin w$" as it can be observed in Eq. (22); this fact implies that the frozen orbits contours are reversed (from $w = \pi/2$ to $w = 3\pi/2$) if the sign of $J_3$ is changed.

Fig. 3 illustrates this region where frozen orbits may exist with $\sin(\Omega - \Omega_\odot) = 0$, $w = \pi/2$ and $w = 3\pi/2$ for the ratio $J_3 = J_2/2$ and sail lightness coefficient $\beta = 0.2$. From these figures, and in order to go into more detail, we fix a constant semimajor axis and plot the level contour sections of $\mathcal{F}$ for low and high altitude orbits.

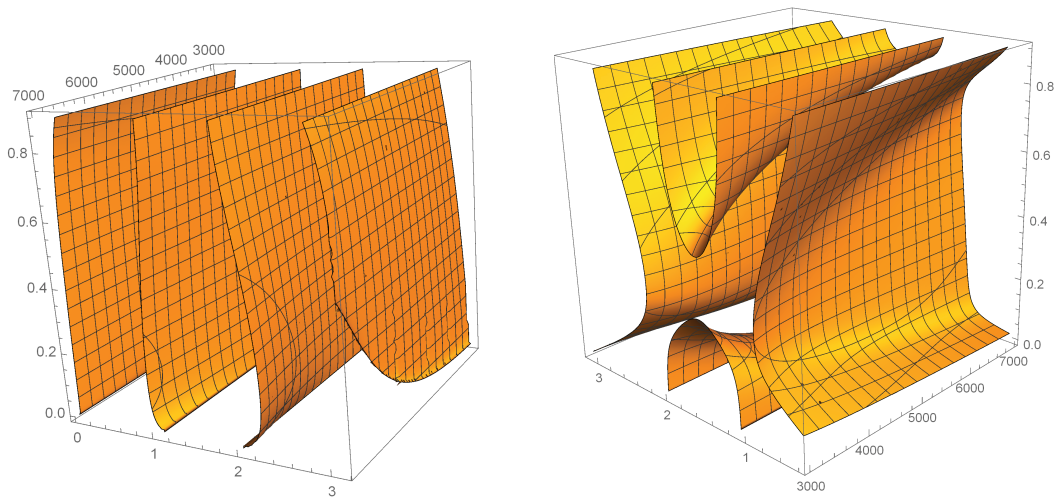


(a) $w = \pi/2$ (b) $w = 3\pi/2$

**Figure 3. The surface $\mathcal{F}(a, e, i)$ of frozen orbits with $J_3 = J_2/2$ and $\beta = 0.2$.**

*1. Low altitude orbits.*

We choose an orbital semimajor axis $a = 3416$[km], which is close to the one of Mercury Planetary Orbiter (MPO), and plot the curves $(i, e)$ for the chosen value of $a$ (see Fig. 4, left). Frozen orbits with periapsis $w = 3\pi/2$ are represented by a solid line, while a dashed one corresponds to $w = \pi/2$. The horizontal line at $e = 0.2858$ is the limit for impact orbits, thus, the orbital eccentricity must be lower than the impact value to a avoid possible collisions with the planet surface. Limiting ourselves to the non-impact region, we observe that the eccentricity of frozen orbits grows when we depart from the equator ($i = 0, \pi$) and approach the critical inclination of the third body for equatorial orbits ($i = 39.2\,^\circ$ as results of vanishing Eq. (33) only for the third body effect). We also observe that there exist frozen orbits at polar inclination, and the eccentricity of these orbits increases when approaching the polar case.

Figure 4 illustrates the behavior of the curves $(i, e)$ of frozen orbits when the sail area to mass ratio varies. We observe that when $\beta$ increases (thickest line), the maximum value of the eccentricity when approaching polar orbits is greater. The opposite behavior occurs at very high eccentricities, for which the minimum value of the eccentricity for the polar case decreases.

Next figure, Fig. 5, depicts a very low-altitude orbit with semimajor axis $a = 2830$[km], note that the maximum allowed eccentricity for non-impact orbits is lower and the eccentricity increases when we approach polar inclinations but do not exist a maximum value corresponding to frozen polar orbits.

*2. High altitude orbits.*

Let us show the frozen orbits location for a high altitude orbit; for this case, we chose a semimajor axis $a = 5612$[km], close to the orbital element of Mercury Magnetospheric Orbiter (MMO). Fig. 6 illustrates the continuous curve of frozen orbits for different values of the eccentricity and inclination. For this semimajor axis, the maximum allowed eccentricity for non-impact orbits is $e = 0.5652$, and frozen polar orbits exhibit a low eccentricity value in the non-impact region. As the orbital altitude increases, the third body and SRP effect increases. This fact is represented as a certain flattening of the curves $(i, e)$ of frozen orbits; as far as the semimajor axis increases the eccentricity of frozen orbits decreases, and it is also observed that the gap between the inclination ranges for $w = \pi/2$ and $w = 3\pi/2$ is reduced and the two lines tend to join near a certain critical inclination. Thence, for high altitude, frozen orbits are almost circular ($e \approx 0$), and the only eccentric frozen orbits are near the critical inclination.

Frozen polar orbits at $w = 3\pi/2$ are represented in Fig. 7; the initial conditions are extracted from Fig. 4 and Fig. 6. We can observe that polar orbits for different values of the eccentricity librate around the corresponding equilibrium points (frozen orbits). Therefore these orbits are suitable orbits for scientific

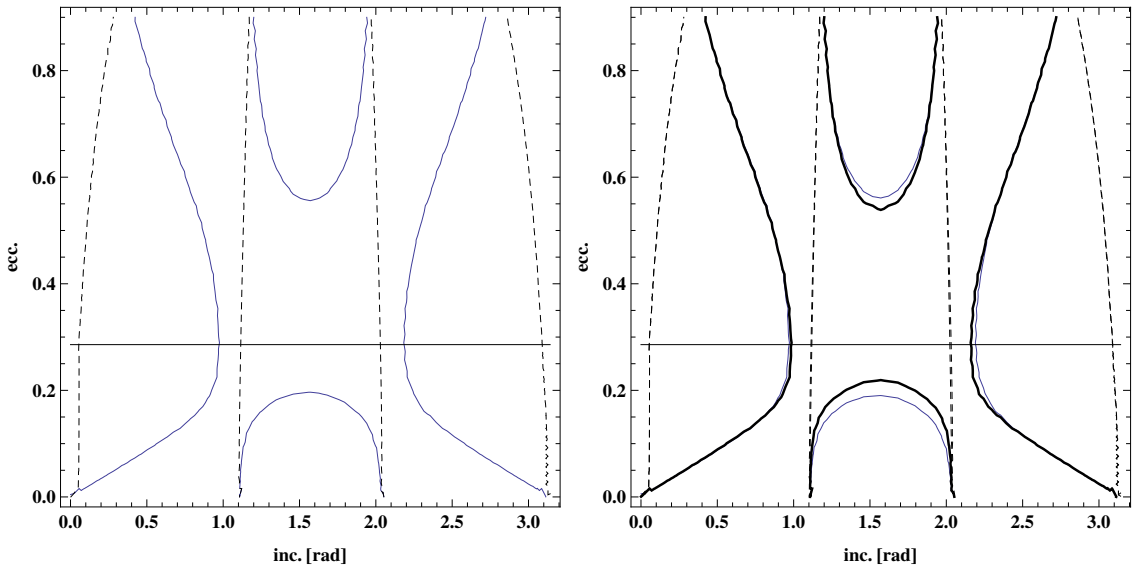


(a) $\beta = 0.2$ (b) $\beta = 0$ and $\beta = 0.8$

**Figure 4. Section $(i, e)$ of frozen orbits with $a = 3416$, $J_3 = J_2/2$ and different values of solar lightness $\beta$. Dashed lines correspond to $w = \pi/2$ and solid lines to $w = 3\pi/2$. In plot on the right, thin solid line corresponds to $\beta = 0$, while the thick solid line is for $\beta = 0.8$.**

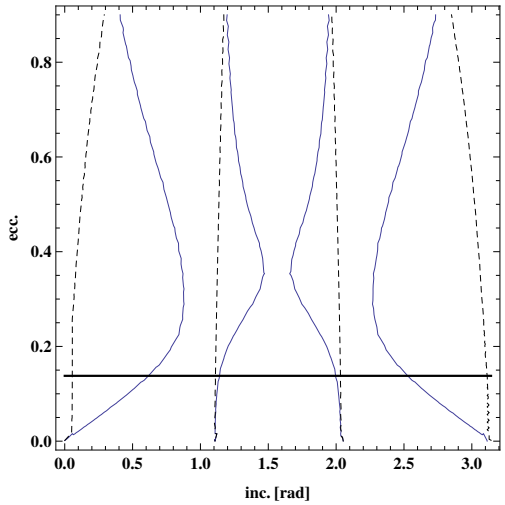


**Figure 5. Section of very low-altitude frozen orbits with $a = 2830$ km, $J_3 = J_2/2$ and $\beta = 0.2$.**

missions about Mercury because they scarcely require control of the orbital eccentricity which leads to the control of the spacecraft lifetime.

It is evident that the symmetry of frozen surfaces is destroyed when the third body has a certain inclination. This asymmetry is more significant when the orbit altitude and the obliquity increase. We observe that the amplitude of a polar frozen orbit at high altitude considerably increases when we include the orbital inclination of the third body (see Fig. 7). However we find that for the case of low altitude orbits, the behavior of the trajectories practically does not change when the inclination is taken into consideration.

It can be seen that although the value of the inclination $i_\odot$ is not high, its effect should not be neglected. Moreover, previous literature[26,27] indicates that the obliquity of the third body orbit could increase the orbital stability due to the fact that it slows down the orbital eccentricity increment.

Finally, we propagate numerically the corresponding initial condition of some of the polar orbits shown in the previous figures for a 100 years interval. Fig. 8 shows the long-term evolution of the eccentricity for a

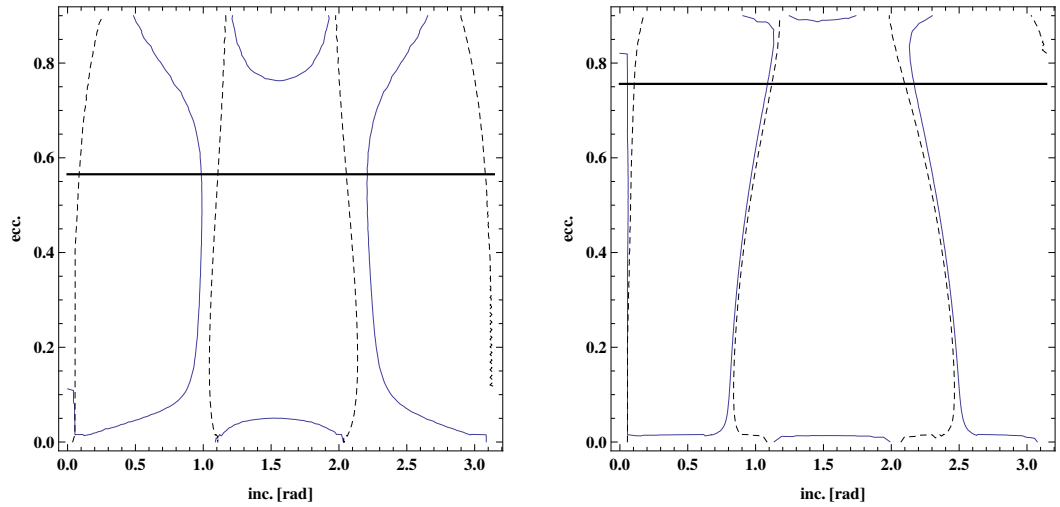


(a) $a = 5612$ (b) $a = 10000$

**Figure 6. Section of high-altitude frozen orbits with $J_3 = J_2/2$ and $\beta = 0.2$.**

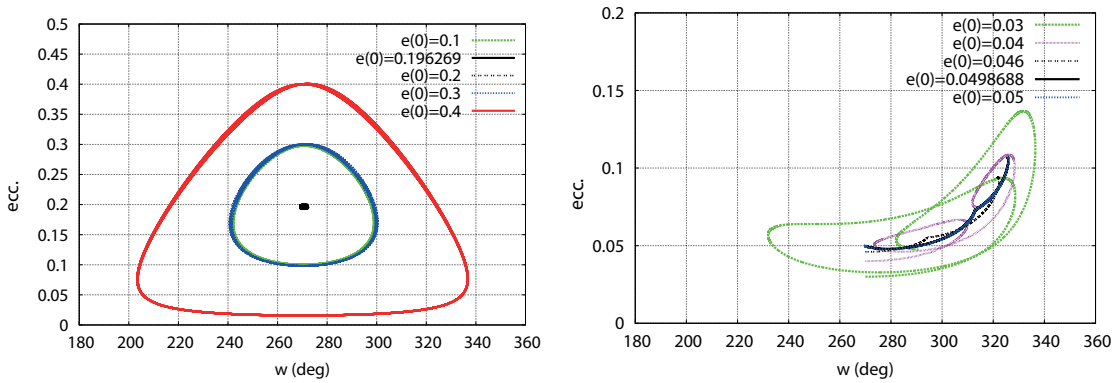


(a) Low-altitude orbit: $a = 3416$ (b) High-altitude orbit: $a = 5612$

**Figure 7. Polar orbits evolution (e,w). Frozen orbits correspond to $e = 0.196269$ and $e = 0.0498688$ respectively.**

sample of two low and two high-altitude polar orbits, one orbit is exactly frozen while the other has orbital elements close to that frozen orbit. The periodic oscillations are due to the averaging process that removes only the secular variations, nevertheless the polar orbits that correspond to $e = 0.196269$ and $e = 0.0498688$ experience less variation due to its frozen character.

Note that the frozen orbits detected correspond to the double-averaged Hamiltonian. The averaged eccentricity and argument of periapsis are a perturbed version of their real correspondents. For a set of initial conditions of a frozen orbit we have performed the numerical propagation to illustrate how these orbits evolve over time. We observe that the frozen character degenerates with time.

Next piece of work is to achieve the averaged Hamiltonian through Lie transforms in order have the generating functions of the involved transformations,[15] and this will allow us to convert the averaged initial condition into osculating elements of the original problem. Another option to recover the frozen condition would be to apply a numerical correction procedure taking the averaged frozen orbits as starters conditions for the complete dynamical model.[16] Previous results show that these initial conditions can be used in the initial system describing the full dynamics (Eq. 9) to generate a good initial guess for frozen orbits.

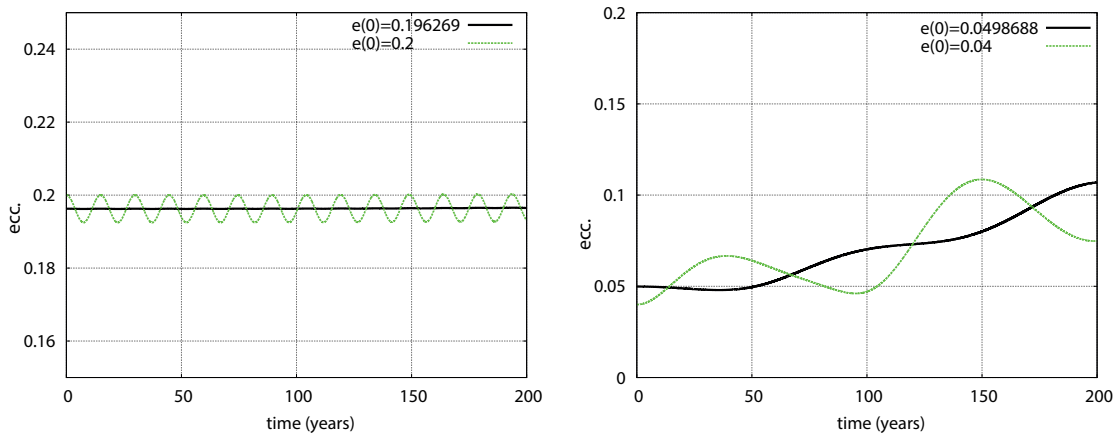


(a) Low-altitude orbit: $a = 3416$ (b) High-altitude orbit: $a = 5612$

**Figure 8. Long-term propagation. Frozen orbits correspond to $e = 0.196269$ and $e = 0.0498688$ respectively.**

## V. Conclusions

This paper has studied the orbital dynamics around Mercury, taking into account the attraction of a third body (Sun) in an elliptical and inclined orbit, as well as solar radiation pressure and the non-uniform distribution of the mass of the planet. We would like to remark that this article did not intend to obtain a complete analytical theory or to study the global dynamics around the planet, but to help in mission designing where frozen orbits are of major interest. With this purpose, solar radiation pressure in the perturbation model has been included in order to visualize the changes in the location of frozen orbits when a solar sailing spacecraft is considered. A double-averaged method has been applied to find a global picture of families of frozen orbits, depending on three parameters: the inclination, the eccentricity and the semimajor axis. Hence, approximate frozen orbits for low and moderate altitudes are obtained.

## Acknowledgments

This research has been funded by the Spanish Ministry of Economy and Competitiveness (code #ESP2013-44217-R). E. Tresaco is grateful for the support of the Centro Universitario de la Defensa de Zaragoza (code #CUD2013-2015). Jean Paulo S. Carvalho is also grateful for the support of CNPq - Brazil (N°306953/2014-5) and the Foundation to Support Research in São Paulo State (FAPESP) (N° 2011/05671-5 and 2012/21023-6) SP-Brazil.

## References

[1]Aliasi, G., Mengali, G., Quarta, A. A., Artificial equilibrium points for a generalized sail in the circular restricted three-body problem Celest Mech Dyn Astr Vol. 110, pp. 343–368, 2011.

[2]Bombardelli, C., and Pelaez, J., On the stability of artificial equilibrium points in the circular restricted three-body problem, Celestial Mechanics and Dynamical Astronomy Vol. 109, pp. 13–26, 2011.

[3]Simo, J. and McInnes, C.R., Displaced solar sail orbits: dynamics and applications. 20th AAS/AIAA Space Flight Mechanics Meeting, 14-17 Feb 2010, San Diego, California, 2010.

[4]Farrés, A., Jorba, A., Periodic and quasi-periodic motions of a solar sail close to $SL_1$ in the Earth-Sun system. Celestial Mechanics and Dynamical Astronomy, Vol. 107, pp. 233–253, 2010.

[5]Gong S. P., Li J. F., Baoyin H. X., Simo, J., A new solar sail orbit. Sci China Tech Sci, Vol. 55, No. 3, pp. 848–855, 2012.

[6]McInnes, C. R., Solar Sailing: Orbital Mechanics and Mission Applications, Advances in Space Research. Vol. 31, No. 8, pp. 1971–1980, 2003.

[7]Scheeres, D.J., Guman, M.D., Villax, B.F., Stability analysis of planetary satellite orbiters: applications to the Europa orbiter. J. Guidance Control Dyn. Vol.24, No. 4, pp.778–787, 2001.

[8]Carvalho, J. P. S., Elipe, A., Vilhena de Moraes, R., Prado, A. F. B. A., Low-altitude, near-polar and near-circular orbits around Europa, Advances in Space Research Vol. 49, No. 5, 994–1006, 2012.

[9]Elipe, A., Lara, M., Frozen orbits about Moon. Journal of Guidance Control and Dynamics. Vol. 26, No. 2, pp. 238–243, 2003.

[10]Carvalho, J. P. dos S., Vilhena de Moraes, R., Prado, A. F. B. A. Some Orbital Characteristics of Lunar Artificial Satellites, Celest. Mech. Dyn. Astron. Vol. 108, No. 4, pp. 371–388, 2010.

[11]Carvalho, J. P. S., Mourão, D. C., Elipe, A., Vilhena de Moraes, R., Prado, A. F. B. A., Frozen orbits around the Europa satellite, Iternational Journal of Bifurcation and Chaos Vol. 22 (10), 1250240, 2012.

[12]Elipe, A., Arribas, M. and T. Kalvouridis, T., Periodic solutions and their parametric evolution in the planar case of the $(n+1)$ ring problem with oblateness. Journal of Guidance, Control and Dynamics, Vol. 30, No. 6, pp. 1640–1648, 2007.

[13]Scheeres, D. J., Satellite dynamics about Asteroids: Computing Poincaré maps for the general case, Hamiltonian Systems with Three or More Degrees of Freedom, NATO ASI Series C, Vol. 533, pp. 554– 557, 1999.

[14]Lara, M., Deprit, A., and Elipe, A., Numerical continuation of families of frozen orbits in the zonal problem of artificial satellite theory. Celestial Mechanics and Dynamical Astronomy Vol. 62, No. 2, pp. 167–181, 1995.

[15]Coffey, S.L., Deprit, A., and Deprit, E. Frozen orbits for satellites close to an Earth-like planet, Celestial Mechanics and Dynamical Astronomy, Vol. 59, No. 1, pp. 32–72, 1994.

[16]Abad, A., Elipe, A., Tresaco E. Analytical Model to Find Frozen Orbits for a Lunar Orbiter, Journal of Guidance, Control, and Dynamics. Vol. 32 (3), pp. 888–898, 2009.

[17]Folta, D., Quinn, D., Lunar frozen orbits, AIAA/AAS Astrodynamics Specialist Conference, Keystone, CO, 2006.

[18]Riaguas, A., Elipe, A., Lara, M., Periodic orbits around a massive straight segment. Celestial Mechanics and Dynamical Astronomy Vol. 73, No. 1-4, pp. 169–178, 1999.

[19]Elipe, A., Lara, M., A simple model for the chaotic motion around (433) Eros. Journal of Astronautical Sciences Vol. 51, No. 4, pp. 391–404, 2003.

[20]Elipe, A., Lara, M., Periodic orbits in the restricted three body problem with radiation pressure. Celestial Mechanics and Dynamical Astronomy Vol. 68, No. 1, pp. 1–11, 1996.

[21]Deprit, A. and Henrard, J. Natural Families of Periodic Orbits, Astronomical Journal, Vol. 72, No. 2, pp. 158–172, 1967.

[22]McInnes, C. R., "Solar Sailing: Technology, Dynamics and Mission Applications", Springer-Praxis Series in Space Science and Technology, Springer-Verlag, 1999.

[23]Smith, David et al. Gravity Field and Internal Structure of Mercury from MESSENGER, Science, Vol. 336, pp. 214-217, 2012.

[24]Delsate, N., Robutel, P., Lemaître, A., Carletti, T., Frozen orbits at high eccentricity and inclination: application to Mercury orbiter, Celest Mech Dyn Astr, Vol. 108, pp. 275-300, 2010.

[25]Lara, M., Palacián, J. F., Yanguas, P., Corral, C. Analytical theory for spacecraft motion about Mercury, Acta Astronautica Vol. 66, pp. 1022–1038, 2010.

[26]Liu, X., Baoyin, H., Ma X. Long-term perturbations due to a disturbing body in elliptic inclined orbit. Astrophysics Space Science, Vol. 339, pp. 295–304, 2012.

[27]Yokoyama, T., Dynamics of some fictitious satellites of Venus and Mars. Planet. Space Sci. Vol. 47, No. 5, pp. 619–627, 1999.